AGE (2007) 29:87–96
DOI 10.1007/s11357-007-9035-y

Neuropathological quantification of dtg APP/PS1: neuroimaging, stereology, and biochemistry

Kebreten F. Manaye · Paul C. Wang · Jahn N. O'Neil · Sophia Y. Huang · Tao Xu · De-Liang Lei · Yousef Tizabi · Mary Ann Ottinger · Donald K. Ingram · Peter R. Mouton

Received: 12 January 2007 / Accepted: 25 May 2007 / Published online: 3 August 2007

Abstract Murine models that mimic the neuropathology of Alzheimer's disease (AD) have the potential to provide insight into the pathogenesis of the disease and lead to new strategies for the therapeutic management of afflicted patients. We used magnetic resonance imaging (MRI), design-based stereology, and high performance liquid chromatography (HPLC) to assess the age-related neuropathology in double transgenic mice that overexpress two AD-related proteins—amyloid precursor protein (APP) and presenilin 1 (PS1)—and age- and gender-matched wild-type (WT) controls. In mice ranging in age from 4–28 months, total volumes of the hippocampal formation (V_{HF}) and whole brain (V_{brain}) were quantified by the Cavalieri-point counting method on a systematic-random sample of coronal T2-weighted MRI images; the same stereological methods were used to quantify V_{HF} and V_{brain} after perfusion and histological processing. To assess changes in AD-type beta-amyloid (Aβ) plaques, sections from the hippocampal formation and amylgdaloid complex of mice aged 5, 12, and 15 months were stained by Congo Red histochemistry. In aged mice with large numbers of amyloid plaques, systematic-random samples of sections were stained by GFAP immunocytochemistry to assess gender and genotype effects on total numbers of astrocytes. In addition, levels of norepinephrine (NE), dopamine (DA), serotonin (5-HT) and 5-HT metabolites were assayed by HPLC in fresh-frozen samples from neocortex, striatum, hippocampus, and brainstem. We confirmed age-related increases in amyloid plaques, beginning with a few plaques at 5 months of age and increasing densities by

K. F. Manaye (✉) · J. N. O'Neil · T. Xu · D.-L. Lei
Department of Physiology and Biophysics,
Howard University College of Medicine,
520 W. Street, NW, Suite 2305,
Adams Bldg., Washington, DC 20059, USA
e-mail: kmanaye@howard.edu

P. C. Wang · S. Y. Huang
Department of Radiology, Howard University
College of Medicine, Washington, DC, USA

Y. Tizabi
Department of Pharmacology, Howard University
College of Medicine, Washington, DC, USA

M. A. Ottinger
University of Maryland, College Park, MD, USA

M. A. Ottinger · D. K. Ingram
Laboratory of Experimental Gerontology,
National Institute on Aging, NIH, Baltimore, MD, USA

D. K. Ingram
Nutritional Neuroscience and Aging Laboratory,
Louisiana State University, Baton Rouge, LA, USA

P. R. Mouton
Stereology Resource Center, Chester, MD, USA

J. N. O'Neil
School of Medicine, Johns Hopkins University,
Baltimore, MD, USA

12 and 15 months. At 15 months of age, there were robust genotype effects, but no gender effects, on GFAP-immunopositive astrocytes in the amygdaloid complex and hippocampus. There were no effects on monoamine levels in all brain regions examined, and no volume changes in hippocampal formation or whole brain as quantified on either neuroimages or tissue sections. Strong correlations were present between volume estimates from MRI images and histological sections, with about 85% reduction in mean V_{HF} or mean V_{brain} between MRI and processed histological sections. In summary, these findings show that the double transgenic expression of AD-type mutations is associated with age-related increases in amyloid plaques and astrocytosis; however, this model does not recapitulate the cortical atrophy or neurochemical changes that are characteristic of AD.

Keywords MRI · Alzheimer's disease · Hippocampal formation · Amygdala · Unbiased stereology

Introduction

About a century ago Alois Alzheimer described neurofibrillary tangles and neuritic plaques in cortical brain regions of a 51-year-old woman with progressive dementia (Alzheimer 1907). Although neuritic plaques and their amyloid components continue to play a critical role in the diagnosis of Alzheimer's disease (AD), semi-quantitative studies in groups of normal-aged and AD patients have reported that these so-called neuropathological markers of AD also occur to varying degrees in cortical tissue during normal aging, and that their accumulation does not directly correlate with the progression of dementia (Mirra et al. 1993; McKeel et al. 2004; Tiraboschi et al. 2004). Stereological and neurochemical studies of brain tissue from patients with AD have confirmed widespread astrocytosis and microgliosis in cortical brain regions and significant reductions in neurotransmitter-specific subcortical nuclei, including the locus coeruleus (LC) and dorsal raphe (DR), and diminished concentrations in their cortical projections of corresponding monoamine neurotransmitters, norepinephrine (NE) and 5-hydroxytrptamine (5-HT); in contrast, these parameters remain relatively stable in brains of persons that undergo normal (non-demented) brain aging (Aletrino et al. 1992; Mouton et al. 1994; Storga et al. 1996; Zarow et al. 2003; Tuppo and Arias 2005). The strongest correlations with dementia severity have been reported in the loss of cortical volume (atrophy), observed by either ante-mortem or post-mortem analyses, and the reduction in cortical synapses (de la Monte 1989; DeKosky and Scheff 1990; Terry et al. 1991; Convit et al. 1993; Jobst et al. 1994; Stout et al. 1996; Mouton et al. 1998; Zarow et al. 2003; de Leon et al. 2004). Thus, the evidence to date indicates that, while the diagnosis of AD depends heavily on the presence of amyloid plaques in neocortical brain regions, the progression of AD dementia appears to correlate more closely with degeneration of subcortical neurotransmitter systems that project to cortex, cortical synapse loss, and reduction of cortical volumes.

The transgenic murine expression of amyloid precursor protein (APP) and presenilin 1 (PS1) human mutation cloned from patients with familial AD results in the deposition of mutant beta-amyloid (Aβ) protein and the formation of amyloid plaques that appear indistinguishable from those in AD (Sze et al. 1997; McGowan et al. 2003). However, no studies have reported on the question of double transgenic (dtg) mice that undergo the progressive cortical atrophy and biochemical degeneration that are characteristic of AD. To address this question we quantified AD-type neuropathology in dtg APP/PS1 mice across the adult mouse lifespan using stereological analyses of ante-mortem neuroimages and post-mortem histological tissue, and neurochemical measurement of NE, dopamine (DA), 5-HT and metabolites by high performance liquid chromatography (HPLC). The results indicate that this line of dtg APP/PS1 mice show some of the neuropathological characteristics associated with AD (amyloid plaque deposition and astrocytosis), but not others (cortical atrophy and reductions in cortical monoamines).

Materials and methods

Mice for these studies were dtg APP/PS1 [Tg (APPswe, PSEN1dE9) 85Dbo, stock #005864] from the Jackson Laboratory (Bar Harbor, Maine, USA) and age- and gender-matched, non-tg, littermate controls (wild-type, WT). At the start of the study all mice weighed between 25 and 28 g and were randomized into dtg APP/PS1 and non-tg groups for

MRI and HPLC (n=13/group) or histology (n=10/group). The age of the 13 mice in the MRI studies spanned the adult lifespan of the mice (4–28 months), with dtg and WT mice matched for age and gender.

MRI Mice were anesthetized with 1.5~2.0 vol% isoflurane mixed with oxygen at a 200 cm^3/min flow rate administered through a nasal cone mask. Mice were placed in the supine position at the center of a Varian 4.7 Tesla NMR machine with 33 cm horizontal magnet bore. A 25-mm long birdcage RF (radio frequency) coil with 20 mm inner diameter was placed around the head of the mouse and used as an RF transmitter and receiver.

High resolution spin echo MRI Spin-echo T2-weighted MRI was used to capture images through the entire brain and hippocampus at scan times of 1.5 h using a 4.7 Tesla NMR machine with the following parameters: repetition time (TR) 2.5 s; echo time (TE) 40 ms; field-of-view 14 mm × 14 mm; and, matrix size 256× 256 pixels. The resulting images had a spatial resolution of 55 μm and a slice thickness of 1 mm. Two sets of 15 images were taken interleavedly through each brain. The total brain volume and hippocampal formation were measured randomly by two investigators hand-drawing the outlines of the regions of interest and then analyzed using the Cavalieri method (Fig. 1). The two investigators were blind to the grouping of the animals. The results were collapsed across age and gender and analyzed for possible transgene effects on V_{HF} and V_{brain}.

Histology Mice were deeply anesthetized via CO_2 inhalation, and then transcardially perfused with phosphate-buffered saline (PBS), 4% paraformaldehyde in 0.1 M PBS (pH 7.4) and postfixed in the 4% paraformaldehyde fixative overnight. The brains were transferred to a 30% sucrose phosphate buffer solution until they sank, then frozen in CO_2/isopentane and stored at −80°C until sectioning. Each brain was serially sectioned in the coronal plane on a sliding freezing microtome. Sections were cut at an instrument setting of 50 μm and sampled in a systematic-random manner, i.e., with random start in the first five sections, then systematic for every fifth section. For estimation of the volume of hippocampal formation (V_{HF}), which included neuronal and molecular layers of DG and CA1-4 regions, sampling was carried out through the entire hippocampus. A similar approach was applied to sampling every tenth section of the total sections through a complete hemisphere for estimation of total brain volume (V_{brain}). Sampled sections were stained using routine cresyl violet (CV) for Nissl substance and cover-slipped for microscopic visualization (Fig. 2). For neurochemistry studies of monoamine concentrations, a separate cohort of mice was sacrificed by cervical dislocation, the brain quickly removed and frozen on powdered dry ice, and stored at −80°C until analysis.

Stereology Using computer-assisted stereology, volumes for MRI slices and tissue sections were estimated using the Cavalieri principle with point counting (Gundersen and Østerby 1981; Gunderson

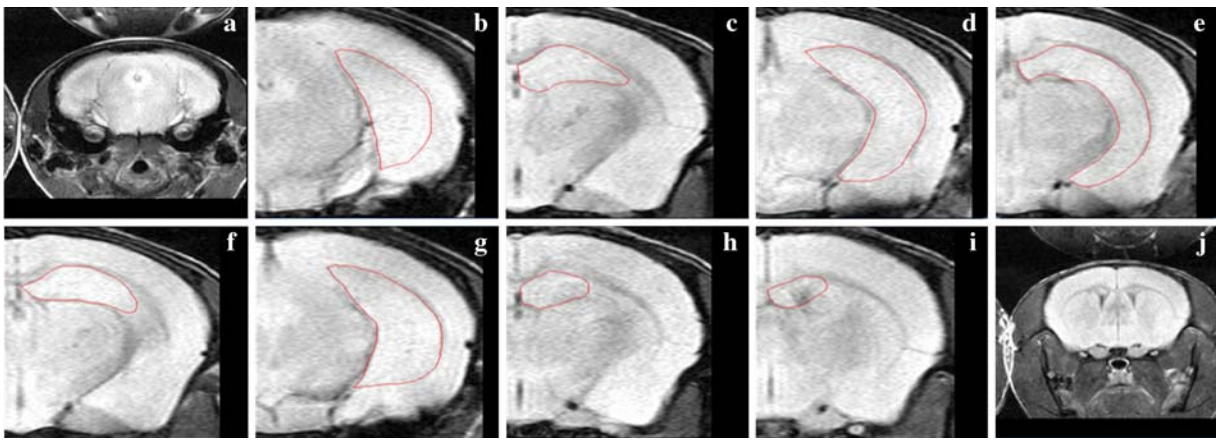

Fig. 1 **a**–**j** Representative T2-weighted MRI of serial sections through the entire mouse hippocampus (*outlined*), with an interslice distance of 1 mm. Note that the first and the last image (shown at lower magnification) do not contain hippocampus

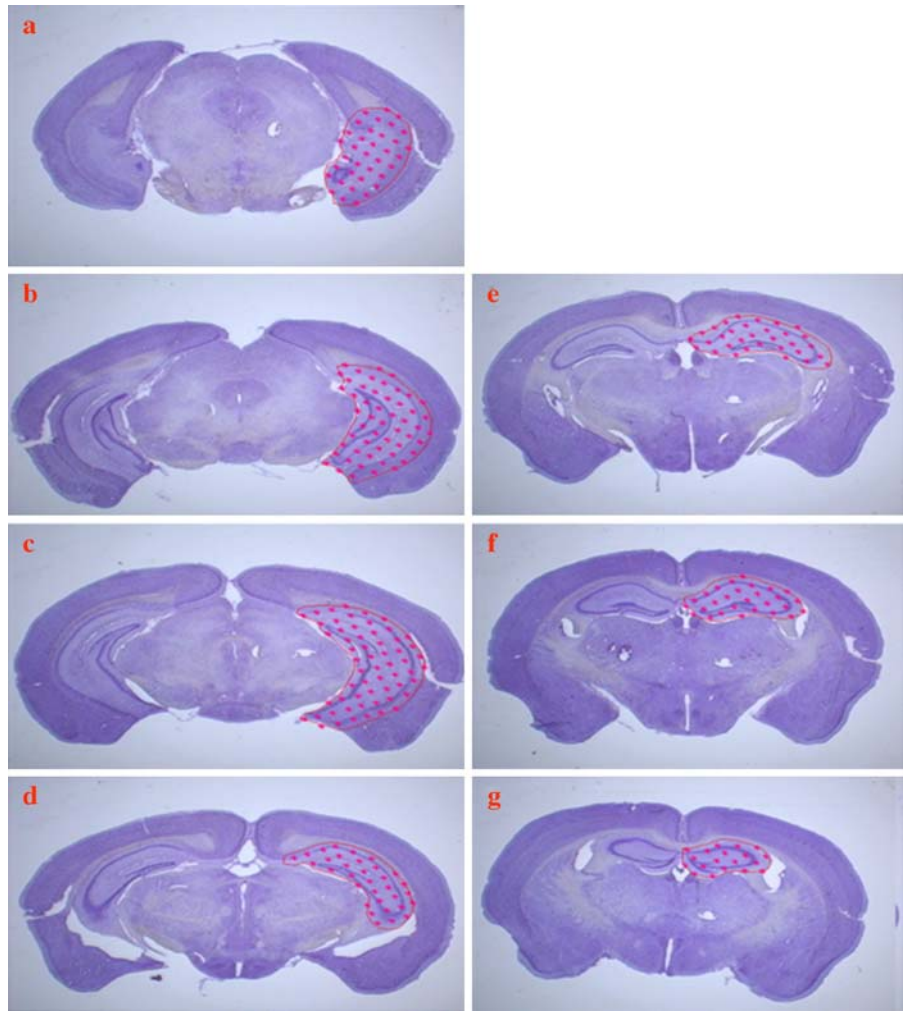

Fig. 2 **a–g** Low power photomicrographs of serial sections through the entire mouse hippocampus; sections were cut at an instrument setting of 50 μm and stained with CV

and Jensen 1987; Long et al. 1998; Gundersen et al. 1999; Roberts et al. 2000; O'Neil et al. in press), as we have detailed previously for brain and hippocampus volumes in human, non-human primate, and rodent brains (de la Monte 1989; Subbiah et al. 1996; Mouton et al. 1997; Mouton 2002; for review Cavalieri 1635 with reprint 1966). The relevant equation for volume estimation: $V_{\text{ref}} = \sum Area_{\text{slices}} \cdot \text{Mean } t$

where,

V_{ref}	Reference volume (hippocampal formation or whole brain, in mm^3)
$\sum Area_{\text{slices}}$	area on slice or section, in mm^2
Mean t	mean post-processing section or slice thickness, mm

In order to capture the majority of variability within- and between-mice for each group, data were collected at a high level of stringency, i.e., the coefficient of error (CE) was less than one-half of the biological variability (Gundersen and Østerby 1981; Long et al. 1998; Gundersen et al. 1999). The results were calculated as mean +/− (SEM) for each group and for each modality (MRI or histology); inter-rater variation between the volumetric measurements was less than 2%. Quantification of total numbers of GFAP-positive astrocytes used the optical disector method, as

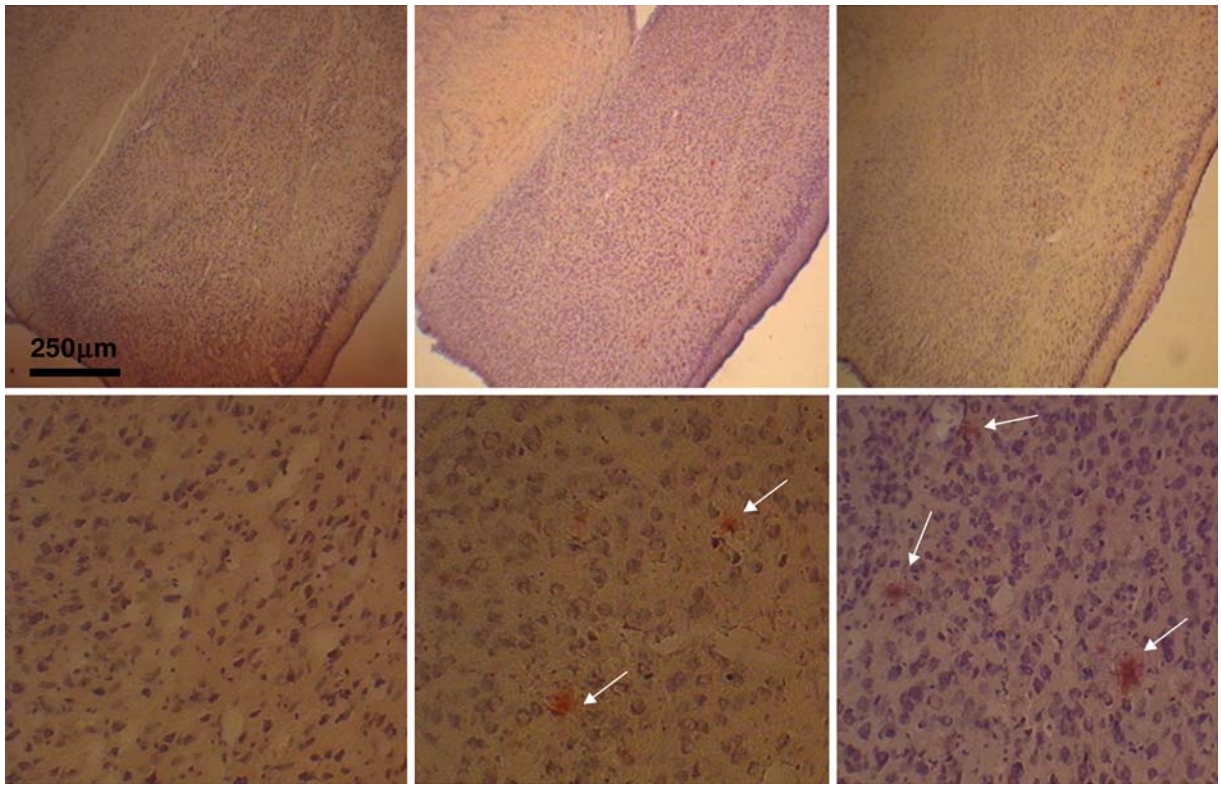

Fig. 3 Congo Red stained sections through the amygdaloid complex of female dtg APP/PS1 mouse brain at increasing ages (from left to right, 5, 12, 16 months of age). Pink staining amyloid-containing plaques present at 12 months, and increase in areal density at 15 months (*white arrows* show amyloid plaques). Magnification bar=250 µm

detailed previously (West 1993; Subbiah et al. 1996; Mouton et al. 1997, 2002; Jankowsky et al. 2003; for review Cavalieri 1635 with reprint 1966).

Monoamine Analyses Due to the stress of MRI procedures, a separate cohort of age-matched mice was sacrificed for analysis of catecholamines and indolamines by HPLC using electrochemical detection (Bioanalytical Systems, West Layfeyette, Indiana, USA). Brains were stored frozen (−80°C) then microdissected regions immediately placed into 0.1M HCl for homogenization. Regions analyzed in this study included the hippocampus, striatum, and cortex. Following homogenization, each sample was centrifuged and filtered (0.2u ACRO, Gelman Sciences, Ann Arbor, Michigan, USA). Samples were assayed individually and kept covered on ice to slow degradation. Monoamines analyzed included NE, DA, 5-HT, and 5-hydroxy-indole-amino acid (5-HIAA). Sample concentrations were calculated against standards that were measured on two channels on the electrochemical detector, which were set at two sensitivities to allow measurement over a greater range of sample concentrations. The software utilized the area under the curve for each standard and unknown for calculations of concentrations. Intra-assay variability was 3–5% and sensitivity was 25–50 pg/sample, with average recovery ranges from 80–90%.

Statistical analysis The groups were analyzed for statistical difference using independent two tailed t-tests; the level for significance was set at $p<0.05$.

Results

Using the Cavalieri-point counting method, V_{HF} and V_{brain} were quantified on systematic-random samples

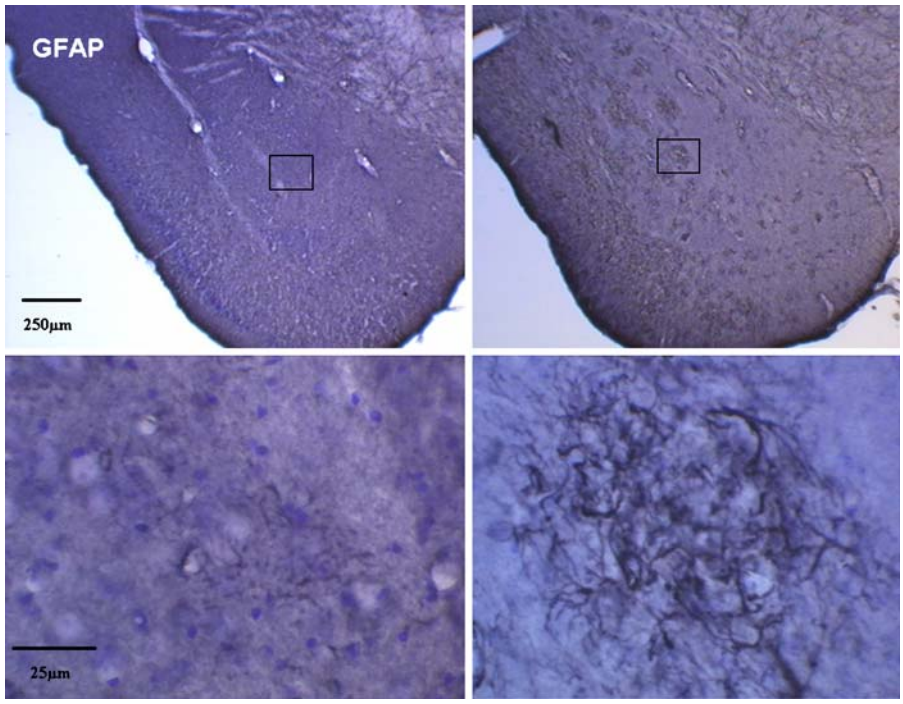

Fig. 4 GFAP-immunostained sections counterstained with CV through amygdaloid complex of 15-month-old female wild-type control (*left*) and dtg APP/PS1 mice (*right*). Note the presence of activated astrocytes in a reticular network around the amyloid deposit at lower right. Magnification bar=25 µm

of MRI images and histology sections from dtg APP/PS1 and WT controls (Figs. 1 and 2). No genotype-based differences were observed in either hippocampus or whole brain volumes from MRI images of dtg APP/PS1 mice [V_{HF}=30.4 (0.12) mm^3, V_{brain}=451.5 (4.31) mm^3, parenthesis represent (SEM)] compared to that for WT controls [V_{HF}=30.7 (0.66) mm^3, V_{brain}=449.6 (0.54) mm^3]. Similarly, the analyses on histological sections revealed no genotype effects on V_{HF} and V_{brain}, with average volumes in the dtg APP/PS1 mice [V_{HF} 4.6 (0.12) mm^3, V_{brain}=61.5 (1.12) mm^3] comparable to that for the WT controls [V_{HF}=4.8 (0.13) mm^3, V_{brain}= 60.2 (2.05) mm^3]. Comparison of the ratio of hippocampus to whole brain volumes [(mean V_{HF}/ mean V_{brain}) •100] showed no differences for volume estimates on MRI images (dtg APP/PS1=6.73% vs. WT=6.83%) or histological sections (dtg APP/PS1=7.48% vs. WT=7.97%). The effects of agonal and tissue processing reduced the average volumes in histological sections by about 84–87% of the same volumes in MRI images.

Congo Red staining of sections showed amyloid deposits in the amygdaloid complex and hippocampus (Figs. 3 and 4), with few deposits at 5 months of age, large numbers by 12 months, and marked increases in densities by 16 months of age. Stereological analysis of total astrocyte numbers in the amygdaloid complex and hippocampus starting at age 15 months revealed significant genotype effects for both males and females (Figs. 5 and 6) compared to age-matched wild-type controls. In the amygdaloid complex this effect was particularly strong, as shown in Fig. 7, with the total number of astrocytes in both male and female dtg APP/PS1 mice more than twice that in the same

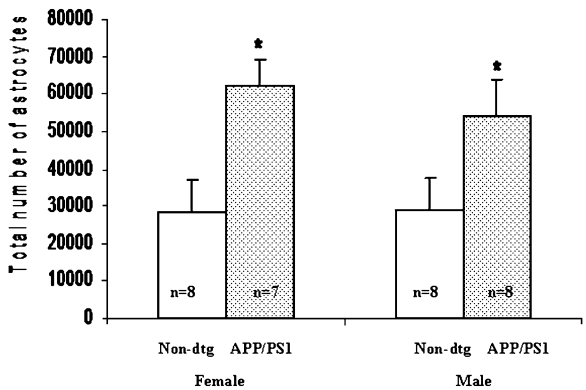

Fig. 5 Stereological counts of mean total numbers of GFAP-immunopositive astrocytes in amygdaloid complex of wild-type and dtg APP/PS1 mice aged 15–23 months (n=7–8/group). *Asterisk* indicates significant genotype effect (p<0.001); there was no significant effect of gender

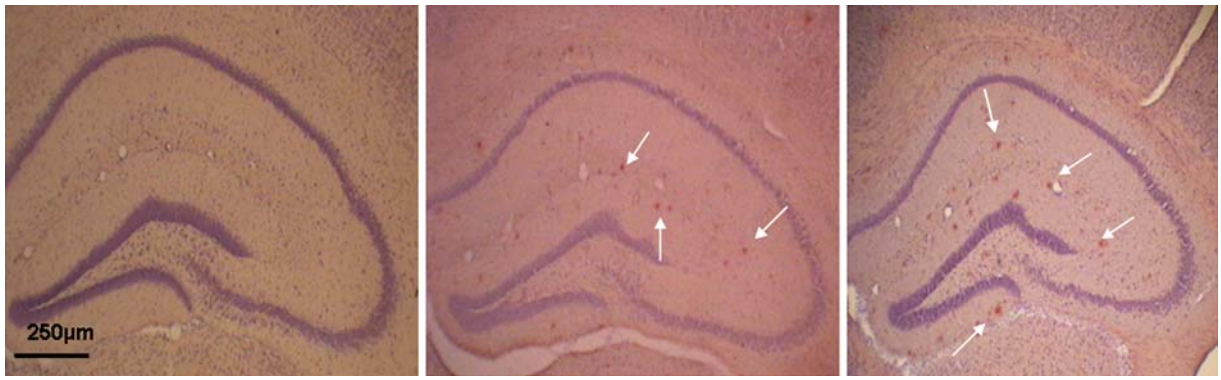

Fig. 6 Congo Red stained sections through hippocampal formation of female dtg APP/PS1 mouse brain at increasing ages. Pink staining amyloid-containing plaques present at 12 months, and increase in areal density at 16 months. Magnification bar=250 μm; *arrows* point to amyloid plaques

regions of age- and gender-matched wild-type controls (Fig. 5). The number of astrocytes increased significantly in hippocampal formation of dtg APP/PS1 compared to age- and gender-matched wild-type controls (Figs. 6 and 8), though this increase was less robust than in the amygdaloid complex.

The results of neurochemistry studies in hippocampus, striatum, or cortex did not reveal any significant differences in monoamine concentrations in brains of dtg APP/PS1 mice compared with values from the same brain regions in age- and gender-matched WT controls.

Discussion

An important criterion for assessing neurodegenerative progression, as seen in AD, is to quantify the neuropathological changes that exist in murine models that overexpress AD-type mutations in relation to those that occur in AD. The present study used neuroimaging, design-based stereology, and HPLC to begin to understand the genotype and gender effects of APP and PS1 co-expression in dtg mice, a strain that forms AD-type amyloid plaques at a much earlier age than single tg APP mice (Jankowsky et al. 2003;

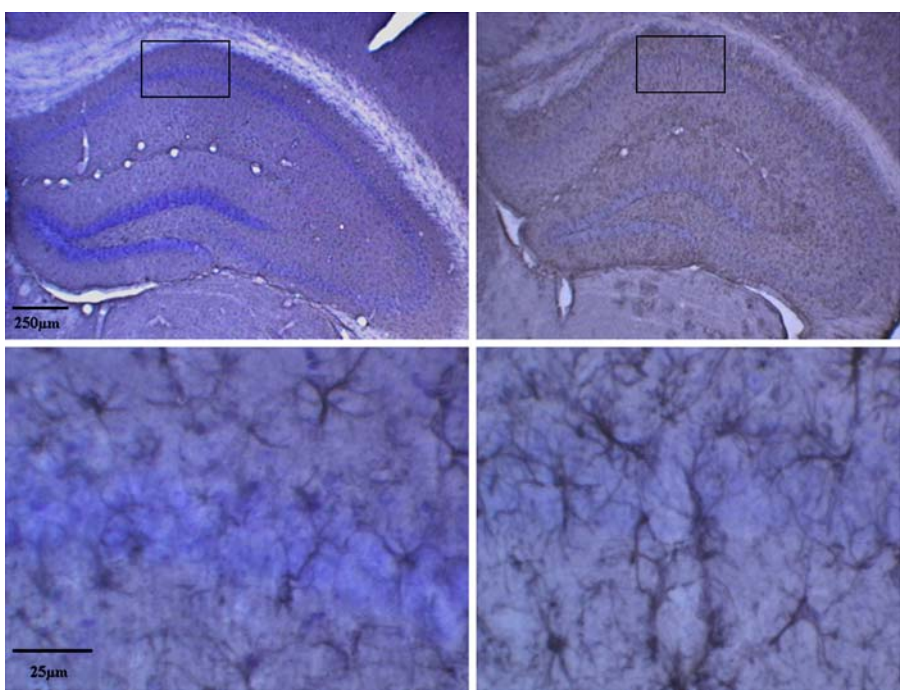

Fig. 7 GFAP-immunostained sections counterstained with CV through hippocampal formation of 15-month-old female wild-eyed control (*left*) and dtg APP/PS1 mice (*right*; at magnification bar=250 μm). Note the presence of activated astrocytes in the layer of CA1 pyramidal neurons at lower right (magnification bar=25 μm). Localization of high magnification image in lower panel indicated by small box in upper panel

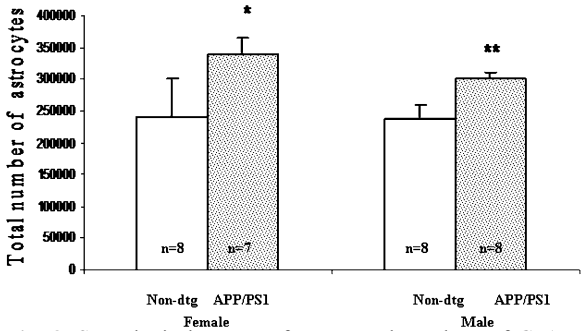

Fig. 8 Stereological counts of mean total numbers of GFAP-immunopositive astrocytes in hippocampal formation of wild-type and dtg APP/PS1 mice aged 15–23 months (n=7–8/group). Asterisks indicate significant genotype effect ($*p<0.01, **p<0.001$); there was no significant effect of gender

McGowan et al. 2003). The findings reported in this study appear to show that dtg APP/PS1 mice manifest certain forms of AD-type neuropathology and fail to manifest others.

The dtg APP/PS1 mice in the present study hyper-accumulate 42 amino acid Aβ residues and Aβ, leading to the earlier appearance of amyloid plaque formation compared to that in single tg APP mice (Jankowsky et al. 2003; McGowan et al. 2003). Sections from age-matched dtg APP/PS1 mice and WT controls were histochemically stained by Congo Red to assess age-related changes in AD-type beta-amyloid (Aβ) plaques. This study confirmed age-related increases in Aβ plaques beginning at 5 months of age and increasing progressively by 12 and 15 months, in agreement with a previous study in a different cohort of the same line of dtgAPPswe/PS1dE9 (Ohno et al. 2006).

Total numbers of GFAP-immunopositive-astrocytes in hippocampal formation and amygdala were quantified by the optical fractionator method. These stereological studies from age 15–23 months confirmed robust astrogliosis in both cortical regions examined, particularly the amygdaloid complex, with no gender effects. With regard to other morphological changes in this strain of dtg APP/PS1 mice, we have previously found evidence of reduced capillary branching at 7 months of age (Lee et al. 2005). We have also reported a significant degeneration in noradrenergic neurons in the LC in dtg APP/PS1 mice at 15 months of age (O'Neil et al. in press). Another study in the same line of dtg APP/PS1 mice (Savenenko et al. 2005), which found no differences in cognitive performance at 6- or 18-months of age, have reported mild decreases in acetylcholinesterase histochemical staining and somatostatin levels in cortex at 18 months of age. Szapacs et al. (2004) reported reduced 5-HT levels in hippocampus at 18 months of age and reduced NE levels at 12- and 18-months of age. In 5-month-old dtg APP/PS1 in this line using a different PS1 mutation (PS1M146V), no differences were found in paired-pulse facilitation (PPF) or post-tetanic potentiation (PTP), two markers of presynaptic component of neurotransmitter release (Szapacs et al. 2004). Thus, neuropathological changes appear to occur in dtg APP/PS1 mice primarily in older age groups.

We found no genotype or gender effects on total volumes of the hippocampal formation (V_{HF}) and whole brain (V_{brain}) quantified either by the stereological method on T1-weighted MRI images or tissue sections after perfusion and histological processing. Since the aim of this study was to quantify total volumes for defined reference spaces, it was not necessary to co-register matched areas on the same coronal level between the MRI images and histological tissues. There were robust quantitative correlations with agonal and tissue-processing changes accounting for ~85% of the differences in cortical and brain volumes in vivo when comparing volume measurements using MRI with the same parameters on cover-slipped histological sections. These robust reductions in mean volumes occurred in both dtg APP/PS1 and wild-type. Brain volumes were quantified at an intermediate step in tissue processing, i.e., after sections were cut, but prior to further tissue processing, which allows the total tissue shrinkage to be partitioned into two components: ~15% shrinkage from agonal effects and the initial steps of tissue processing (fixation and sectioning), and ~70% volume loss during the final steps of tissue processing for microscopic visualization (i.e., dehydration, cresyl violet histochemistry, and coverslipping). The close correspondence in the ratios of hippocampal to whole brain volumes on MRI images and histological sections, along with inter-rater variation of the volumetric measurement of less than 2%, confirms the reliability of the technique for quantification of volumes. Finally, these comparable ratios indicate that the methods for immobilization and monitoring of cardiac and respiratory function did not blur the MRI images enough to confound the quantification process.

Another important goal of this research is to investigate the potential of ante-mortem neuroimaging

of Aβ-containing plaques in cortical brain regions to assist in the early clinical diagnosis of AD (Convit et al. 1993; Benveniste et al. 1999; Dedeoglu et al. 2004). Previous studies using T1ρ("T-1-rho")-weighted MRI have been moderately successful in demonstrating Aβ-containing plaques in vivo based on local variations in protein content (Poduslo et al. 2002). Enhanced visualization of amyloid plaques in dtg APP/PS1 mice has been demonstrated by pre-injecting Aβ peptides magnetically labeled with gadolinium or iron oxide nanocrystals (Borthakur et al. 2003). A recent MRI study of dtg APP/PS1 mice reported differences with respect to non-tg controls in the transverse relaxation time *T*2, in several regions of cortical grey matter (hippocampus, cingulate, and retrosplenial cortex), which may reflect impaired cell physiology in these regions (Wadghirii et al. 2003). The absence of differences in T1-weighted or proton density weighted MRI images suggests that heavily T2-weighted images may be more sensitive to amyloid accumulation in the dtg APP/PS1 mice (Helpern et al. 2004).

In summary, this line of dtg APP/PS1 mice show several morphological changes associated with AD, including age-related increases in amyloid plaques, astrocytosis, and LC degeneration, and fail to recapitulate the loss of cortical volume and reductions in cortical monoamine concentrations that characterize AD. Among the possible explanations for this observation is the likelihood that compensatory sprouting of serving LC neurons occurs in those mice to ensure neurochemical innervation to all main areas; in AD, similar compensation may occur until the final stage of the disease prior to death. Our studies will continue to develop the optimal MRI parameters to visualize ligands that effectively cross the blood brain barrier and bind to microscopic targets associated with AD neuropathology. Further cross-sectional and time-course studies are needed to help build a stronger view of the neuropathological profile in the brains of these mice with respect to the neuropathology associated with AD.

Acknowledgements The authors would like to recognize the Public Health Service for funding support for these studies (SNRP2U54NS039407-06, NIH grant MH076541-02A1, RCMI/NCRR/NIH G12RR03048, US Army USAMRMC W81XWH-05-1-0291, NIH MHIRT 9T 37-MD001582-08) and the technical support of Armand Oei and Huafu Song in the laboratory of Biomedical NMR at the Howard University School of Medicine. The authors also appreciate the support of Nikki Thompson for the monoamine assays through the Maryland Agriculture Experiment Station of the University of Maryland.

References

Aletrino MA, Vogels OJ, Van Domburg PH, Ten Donkelaar HJ (1992) Cell loss in the nucleus raphe dorsalis in Alzheimer's disease. Neurobiol Aging 13(4):461–468

Alzheimer A (1907) Ueber eine eigenartige Erkrankung der Hirnrinde. Allgemeine Zeitschrift fur Psychiatrie 64:146–148

Benveniste H, Einstein G, Kim KR, Hulette C, Johnson GA (1999) Detection of neuritic plaques in Alzheimer's disease by magnetic resonance microscopy. Proc Natl Acad Sci USA 96(24):14079–14084

Borthakur A, Urya K, Chively SB, Poptani H, Corbo M, Charagundla SR, Trojanoqski JQ, Lee VM, Reddy R (2003) In Vivo T_1 weighted MRI of amyloid transgenic mouse model of Alzheimer's disease. Proc Intl Soc Mag Reson Med 11:2039

Cavalieri B (1635) Geometria indivibilibus continuorum. Bononi: Typis Clementis Ferronij. Reprint from (1966) Geometria degli indivisibili. Torino: Unione Tipografico-Editrice Torinese

Convit A, de Leon MJ, Golomb J, George AE, Tarshish CY, Bobinski M, Tsui W, De Santi S, Wegiel J, Wisniewski H (1993) Hippocampal atrophy in early Alzheimer's disease: anatomic specificity and validation. Psychiatr Q 64:371–387

Dedeoglu A, Choi JK, Cormier K, Kowall NW, Jenkins BG (2004) Magnetic resonance spectroscopic analysis of Alzheimer's disease mouse brain that express mutant APP shows altered neurochemical profile. Brain Res 1012(1–2):60–65

DeKosky ST, Scheff SW (1990) Synapse loss in frontal cortex biopsies in Alzheimer's disease: correlation with cognitive severity. Ann Neurol 27:457–464

de la Monte SM (1989) Quantitation of cerebral atrophy in preclinical and end-stage Alzheimer's disease. Ann Neurol 25:450–459

de Leon MJ, DeSanti S, Zinkowski R, Mehta PD, Pratico D, Segal S, Clark C, Kerkman D, DeBernardis J, Li J, Lair L, Reisberg B, Tsui W, Rusinek H (2004) MRI and CSF studies in the early diagnosis of Alzheimer's disease. J Intern Med 256:205–223

Gunderson HJ, Jensen EB (1987) The efficiency of systematic sampling in stereology and its prediction. J Microsc 147(Pt 3):229–263

Gundersen HJG, Jensen EV, Kieu K, Nielsen J (1999) The efficiency of systematic sampling in stereology - revisited. J Microsc 193:199–211

Gundersen HJG, Østerby R (1981) Optimizing sampling efficiency of stereological studies in biology: or "Do more less well." J Microsc 121:65–73

Helpern JA, Lee S-P, Falangol MF, Dyakin VV, Bogart A, Ardekani B, Duff K, Branc C, Wisniewski T, de Leon MJ, Wolf O, O'Shea J, Nixon RA (2004) MRI assessment of neuropathology in a transgenic mouse model of Alzheimer's disease. Magn Reson Med 51:794–798

Jankowsky J, Fadale DJ, Andersen JK, Xu G, Gonzales V, Jenkins NA, Copeland NG, Lee MK, Younkin LH, Wagner SL, Younkin SG, Borchelt DR (2003) Mutant presenilins specifically elevate the levels of the 42 residue beta-amyloid peptide in vivo: evidence for augmentation of a 42-specific gamma secretase. Hum Mol Genet 13(2):159–170

Jobst KA, Smith AD, Szatmari M, Esiri MM, Jaskowski A, Hindley N, McDonald B, Molyneux AJ (1994) Rapidly progressing atrophy of medial temporal lobe in Alzheimer's disease. Lancet 343:829–830

Lee GD, Aruna JH, Barrett JM, Lei D-L, Ingram DK, Mouton PR (2005) Stereological analysis of microvascular parameters in a double transgenic model of Alzheimer's disease. Brain Res Bull 65:317–322

Long JM, Kalehua AN, Muth NJ, Calhoun ME, Jucker M, Hengemihle JM, Ingram DK, Mouton PR (1998) Stereological analysis of astrocyte and microglia in aging mouse hippocampus. Neurobiol Aging 19:497–503

McGowan E, Pickford F, Dickson DW (2003) Alzheimer animal models: models of Aβ deposition in transgenic mice. In: Dickson DW (ed) Neurodegeneration: the molecular pathology of dementia and movement disorders. ISN Neuropath Press, Basel, pp 74–79

McKeel DW, Price JL, Miller JP, Grant EA, Xiong C, Berg L, Morris JC (2004) Neuropathologic criteria for diagnosing Alzheimer disease in persons with pure dementia of Alzheimer type. J Neuropathol Exp Neurol 63(10):1028–1037

Mirra S, Hart MH, Terry RD (1993) Making the diagnosis of Alzheimer's disease. A primer for practicing pathologists. Arch Pathol Lab Med 117:132–144

Mouton PR (2002) Principles and practices of unbiased stereology: an introduction for bioscientists. Johns Hopkins University Press, Baltimore

Mouton PR, Long JM, Lei DL, Howard V, Jucker M, Calhoun ME, Ingram DK (2002) Age and gender effects on microglia and astrocyte numbers in brains of mice. Brain Res 956(1):30–35

Mouton PR, Martin LJ, Calhoun ME, Dal Forno G, Price DL (1998) Cognitive decline strongly correlates with cortical atrophy in Alzheimer's dementia. Neurobiol Aging 19: 371–377

Mouton PR, Pakkenberg B, Gundersen HJG, Price DL (1994) Absolute number and size of pigmented locus coeruleus neurons in the brains of young and aged individuals. J Chem Neuroanat 7:185–190

Mouton PR, Price DL, Walker LC (1997) Empirical assessment of synapse numbers in primate neocortex. J Neurosci Methods 75:119–126

Ohno M, Chang L, Tseng W, Oakley H, Citron M, Klein WL, Vassar R, Disterhoft JF (2006) Temporal memory deficits in Alzheimer's mouse models: rescue by genetic deletion of BACE1. Eur J Neurosci 23(1):251–260

O'Neil JN, et al. Catecholaminergic neuronal loss in locus coeruleus of aged female dtg APP/PS1 mice. J Chem Neuroanat (in press)

Poduslo JF, Wengenack TM, Curran GL, Wisniewski T, Sigurdsson EM, Macura SI, Borowski BJ, Jack CR Jr (2002) Molecular targeting of Alzheimer's amyloid plaques for contrast-enhanced magnetic resonance imaging. Neurobiol Dis 11(2):315–329

Roberts N, Puddephat MJ, McNulty V (2000) The benefit of stereology for quantitative radiology. Br J Radiol 73 (871):679–697

Savenenko A, Xu GM, Melnikova T, Morton J, Gonzales V, Wong M, Price DL, Tang F, Markowska AL, Borchelt DR (2005) Episodic-like memory deficits in the APPswe/PS1dE9 mouse model of Alzheimer's disease: relationship to β-amyloid deposition and neurotransmitter abnormalities. Neurobiol Dis 18(3):602–617

Storga D, Vrecko K, Birkmayer JG, Reibneggar G, Cavalieri B (1996) Monoaminergic neurotransmitters, their precursors and metabolites in brains of Alzheimer patients. Neurosci Lett 203(1):29–32

Stout JC, Jernigan TL, Archibald SL, Salmon DP (1996) Association of dementia severity with cortical gray matter and abnormal white matter volumes in dementia of the Alzheimer type. Arch Neurol 53:742–749

Subbiah P, Mouton PR, Fedor H, McArthur JC, Glass JD (1996) Stereological analysis of cerebral atrophy in human immunodeficiency virus-associated dementia. Exp Neurol 55(10):1032–1037

Szapacs ME, Numis AL, Andrews AM (2004) Late onset loss of hippocampal 5-HT and NE is accompanied by increases in BDNF protein expression in mice co-expressing mutant APP and PS1. Neurobiol Dis 16(3):572–580

Sze CI, Troncoso JC, Kawas C, Mouton PR, Price DL, Martin LJ (1997) Loss of the presynaptic vesicle protein synaptophysin in hippocampus correlates with cognitive decline in Alzheimer disease. J Neuropathol Exp Neurol 56(8):933–944

Terry RD, Masliah E, Salmon DP, Butters N, DeTeresa R, Hill R, Hansen LA, Katzman R (1991) Physical basis of cognitive alterations in Alzheimer's disease: synapse loss is the major correlate of cognitive impairment. Ann Neurol 30:572–580

Tiraboschi P, Hansen LA, Thal LJ, Corey-Bloom J (2004) The importance of neuritic plaques and tangles to the development and evolution of AD. Neurology 64:1984–1989

Tuppo EE, Arias HR (2005) The role of inflammation in Alzheimer's disease. Int J Biochem Cell Biol 37(2):289–305

Wadghirii YZ, Sigurdsson EM, Sadowski M, Elliott JI, Li Y, Scholtzova H, Tang Cy, Aguinaldo G, Pappolla M, Duff K, Wisniewski T, Turnbull DH (2003) Detection of Alzheimer's amyloid in transgenic mice using magnetic resonance microimaging. Magn Reson Med 50(2): 293–302

West MJ (1993) Regionally specific loss of neurons in the aging human hippocampus. Neurobiol Aging 14(4):287–293

Zarow C, Lynness SA, Mortimer JA, Chui HC (2003) Neuronal loss is greater in the locus coerulus than nucleus basalis and substantia nigra in Alzheimer and Parkinson diseases. Arch Neurol 60(3):337–341